Pharm Res (2014) 31:160–172
DOI 10.1007/s11095-013-1149-6

RESEARCH PAPER

Molecular Basis of Crystal Morphology-Dependent Adhesion Behavior of Mefenamic Acid During Tableting

Vrushali Waknis • Elza Chu • Roxana Schlam • Alexander Sidorenko • Sherif Badawy • Shawn Yin • Ajit S. Narang

Received: 3 January 2013 / Accepted: 16 July 2013 / Published online: 14 August 2013
© Springer Science+Business Media New York 2013

ABSTRACT

Purpose The molecular basis of crystal surface adhesion leading to sticking was investigated by exploring the correlation of crystal adhesion to oxidized iron coated atomic force microscope (AFM) tips and bulk powder sticking behavior during tableting of two morphologically different crystals of a model drug, mefenamic acid (MA), to differences in their surface functional group orientation and energy.

Methods MA was recrystallized into two morphologies (plates and needles) of the same crystalline form. Crystal adhesion to oxidized iron coated AFM tips and bulk powder sticking to tablet punches was assessed using a direct compression formulation. Surface functional group orientation and energies on crystal faces were modeled using Accelrys Material Studio software.

Results Needle-shaped morphology showed higher sticking tendency than plates despite similar particle size. This correlated with higher crystal surface adhesion of needle-shaped morphology to oxidized iron coated AFM probe tips, and greater surface energy and exposure of polar functional groups.

Conclusions Higher surface exposure of polar functional groups correlates with higher tendency to stick to metal surfaces and AFM tips, indicating involvement of specific polar interactions in the adhesion behavior. In addition, an AFM method is identified to prospectively assess the risk of sticking during the early stages of drug development.

KEY WORDS adhension · atomic force microscopy · mefenamic acid · morphology · surface energy

V. Waknis • R. Schlam • S. Badawy • S. Yin • A. S. Narang (✉)
Bristol-Myers Squibb, Co., One Squibb Dr.
New Brunswick, New Jersey 08901, USA
e-mail: ajit.narang@bms.com

E. Chu • A. Sidorenko
Department of Chemistry and Biochemistry
University of the Sciences, Philadelphia, Pennsylvania 19104, USA

ABBREVIATIONS

AFM	Atomic force microscopy
API	Active pharmaceutical ingredient
EtOH	Ethanol
MA	Mefenamic acid
PoF	Pull-off-force
PSD	Particle size distribution
PXRD	Powder X-ray diffraction
SEM	Scanning electron microscopy
THF	Tetrahydrofuran
XRD	X-ray diffraction

INTRODUCTION

Crystalline drugs are commonly used in the manufacture of oral solid dosage forms, such as tablets. The manufacturability of these dosage forms is highly dependent on bulk properties of the active pharmaceutical ingredient (API) – such as flow, compactibility, and sticking. Bulk properties refer to phenomena generally observed when a large number of crystals, typically in a formulation, are involved in a bulk powder handling unit operation – ranging in powder amounts from several hundred grams to kilograms. The sticking behavior is a manifestation of API adhesion to steel surfaces, commonly utilized in pharmaceutical processing, followed by material buildup; especially in high drug load formulations. The influence of API molecular structure and its configuration in crystal unit cell on its bulk properties occurs on the microscale and depends on the micromeritics of drug crystals – *i.e.*, particle size, shape, and morphology. For example, flow and density of bulk powder is a known function of the crystal form, size, and shape (1). However, the fundamental mechanisms behind the phenomenon of metal adhesion leading to sticking are not well understood. A mechanistic understanding of the dependence of bulk properties of drug substance and drug

product on the morphological and surface characteristics of the API crystals is expected in the contemporary and evolving quality-by-design (QbD) paradigm of drug product development. In addition, such fundamental knowledge would facilitate the development and use of material sparing techniques during the early stage of drug product and process development to identify potential risks and mitigation strategies.

The vast majority of organic crystals are anisotropic. The anisotropy is caused by differences in surface exposure and/or orientation of functional groups of a molecule in the crystal structure. The solvent(s) used for crystallization have an impact on the morphology of resulting crystals (2–4). For example, greater supersaturation generally leads to smaller sized crystals due to higher rate of nucleation (5). Differences in the relative growth rate of crystal faces as a function of the degree of supersaturation contributes to differences in crystal shape (6). Crystal shape is dominated by faces that have the lowest growth rate (7). In addition, specific crystal-solvent interactions during crystal formation can influence the relative growth rate of different crystal faces. Thus, while studying the morphological sensitivity to the solvent phase and purity, Braybrook *et al.* observed that copper (II) acetate monohydrate crystals grown from propran-1-ol yielded needle-shaped morphology, whereas the use of aqueous media resulted in orthodrome-shaped crystals (8). Morphological differences were attributed to crystal/solvent interactions during crystal formation. The authors proposed that the appearance of the (100) faces in the needle-shaped morphology was related to the ability of propan-1-ol to adsorb to the designated crystal surfaces mediated by the binding of the solvent hydroxyls to the lattice water molecules *via* hydrogen bonding. Holmback and Rasmuson studied the influence of precipitant addition rate on the morphology of benzoic acid crystals produced from saturated ethanol/water solutions (7). The authors observed that the crystal habit changes from needle-like particles to platelets by increasing the ethanol bulk concentration. Utilizing attachment-energy modeling, the authors concluded the surface exposure and orientation of carboxylate functional groups were important determinants of intermolecular interaction with the solvent, thus reducing the relative growth rate and surface area of different faces in the resulting crystal morphology.

Crystal anisotropy often results in variances in the measurable properties of different faces of the crystals. For example, Heng *et al.* observed differences in the wettability of various crystallographic faces of aspirin single crystals, which correlated to differences in the surface exposure of carboxylic acid groups and surface energy of the faces (9). The authors noted similar observation for acetaminophen and ibuprofen crystals (10). The differences in the surface group orientation and polarity of crystal faces can affect properties that are influenced by the functional group interaction at the solid surface. For example, Danesh *et al.* reported a correlation of surface exposure of benzene rings *versus* ester groups with six-fold difference of dissolution between two faces of aspirin crystals (11). Crystal morphology determines the relative surface area of various faces of a crystal, which can affect surface dependent phenomena of morphologically different forms of a drug. Some pharmaceutical processes, such as tableting, involve multiple contacts of the bulk powder with the punch surface under high pressure. Thus, the phenomenon of sticking is likely to comprise cumulative forces of adhesion arising from multiple interactions of surface exposed functional groups.

Sticking is a well-known but complex problem in the manufacture of oral solid dosage forms. It is encountered in bulk powder processing, often only at large scale. Not only is the occurrence of this phenomenon drug substance specific, it further depends upon the polymorphic form and morphology/shape of drug crystals. The complex nature of this phenomenon makes it unpredictable and highly variable. It poses significant risk to the developability and manufacturability of drug product. Therefore, there is a significant unmet need for identifying and establishing small-scale experimental and molecular modeling tools to prospectively assess the sticking risk for new drug candidates' morphologies and crystal forms. Mechanistically, nonspecific and weak but multiple van der Waals forces of attraction between the API and the metal surface acting over a prolonged time (*e.g.*, added dwell time of multiple tablet compression) are generally thought to be responsible for the sticking phenomenon. However, the sticking tendency is generally greater when the metal surface is oxidized (*e.g.*, rusting of punches used for tablet compression) and increases with environmental humidity.

Therefore, we hypothesize that the mechanism of sticking would involve stronger forces and specific interactions that require surface exposure of electronegative atoms and/or polar functional groups on drug crystals. In this work, we test this hypothesis by molecular modeling combined with the assessment of relative adhesion of two morphologies of a model drug (mefenamic acid, MA) to an oxidized iron coated tip by atomic force microscopy (AFM) (Fig. 1). Several studies have explored the use of AFM as an experimental tool to assess the risk of sticking in crystalline drugs. Some investigators have modified AFM probe tips by attaching single crystals (*e.g.*, with a glue that is cured by UV radiation (12)) to measure drug crystal adhesion to a tablet punch surface. Bunker *et al.* utilized this approach to study the force of adhesion between lactose crystals and punch surfaces of differing roughness and under different relative humidities (13). Not only are the mounting and adhesion of crystals on the AFM tips tedious, multiple measurements of several crystals using these tips require the assumption of isotropic adhesion to different crystal faces. Furthermore, this method measures adhesion forces at one location on a single mounted crystal. For a method to be useful for prediction of sticking tendency of crystalline powders, adhesion forces across

different faces of the several crystals should be quantified. Non-functionalized AFM tips have also been used to study the surface adhesion behavior of drug crystals. For example, Wang *et al.* investigated the work of adhesion between ketoprofen, ibuprofen, and flurbiprofen using iron coated tips in a contact mode AFM study (14). The rank order of work of adhesion between iron and profen compounds was correlated to the rank order of interaction between drug molecules and iron superlattices predicted by molecular simulation. The work of adhesion between the AFM tip and the drug molecules was studied by melting and recrystallization of drug molecules into a flat surface, and measurements were carried out while both the probe tip and the profen surface were immersed in a saturated solution of the drug in water to stabilize the surface of the crystal. Although the authors obtained correlation of AFM force of adhesion measurements with molecular modeling predictions, the experimental conditions of recrystallization and immersion in saturated solution would limit robust correlation of data generated using this technique with sticking observation in dry powder state, *e.g.*, during tableting. To overcome some of the limitations in the AFM studies reported in the literature, oxidized Fe-coated tips were used for adhesion force measurement from multiple crystals of either morphology in this study.

MA is known to exhibit propensity for sticking during tablet compression (15). In addition to relative adhesion of the two morphologies to oxidized iron coated AFM tips, a correlation of sticking tendency and AFM findings with the surface exposure of functional groups and surface energy of the two crystal forms was investigated. MA was crystallized into two different morphologies (shapes), while maintaining the same crystalline polymorphic form (form I). The morphologies were characterized for particle size distribution, relative sticking tendency during tablet compression, and adhesion to oxidized iron coated tips by AFM. In addition, the surface exposure of functional groups for the two morphologies was modeled, and the surface free energy was calculated. The AFM pull-off forces (PoF) were correlated to the sticking tendency of the two morphologies. This work identified AFM as a potential small-scale predictive method to assess the risk of sticking early in drug development. The correlation of surface exposure of functional groups and surface free energy of the two morphologies to the sticking tendency was used to identify molecular mechanisms responsible for the sticking tendency.

MATERIALS AND METHODS

Materials

Mefenamic acid (MA) was procured from Sigma Aldrich (Sigma-Aldrich, St. Louis, MO). Solvents tetrahydrofuran (THF), ethanol (EtOH), and hexane (all high performance liquid chromatography grade) were also obtained from Sigma Aldrich.

Methods

Recrystallization

Plate-shaped crystals were obtained by preparing a saturated solution of MA in THF at 40°C, followed by slow solvent evaporation at 5–10°C. The plate-shaped crystals were filtered after 4 h, washed with water, dried in a vacuum chamber, and stored in tightly closed containers at room temperature.

Needle-shaped crystals were obtained by preparing a saturated warm solution of MA in a 1:1 v/v mixture of THF and EtOH, to which 5 parts hexane was added as an anti-solvent. The needle-shaped crystals were filtered after 4 h, washed

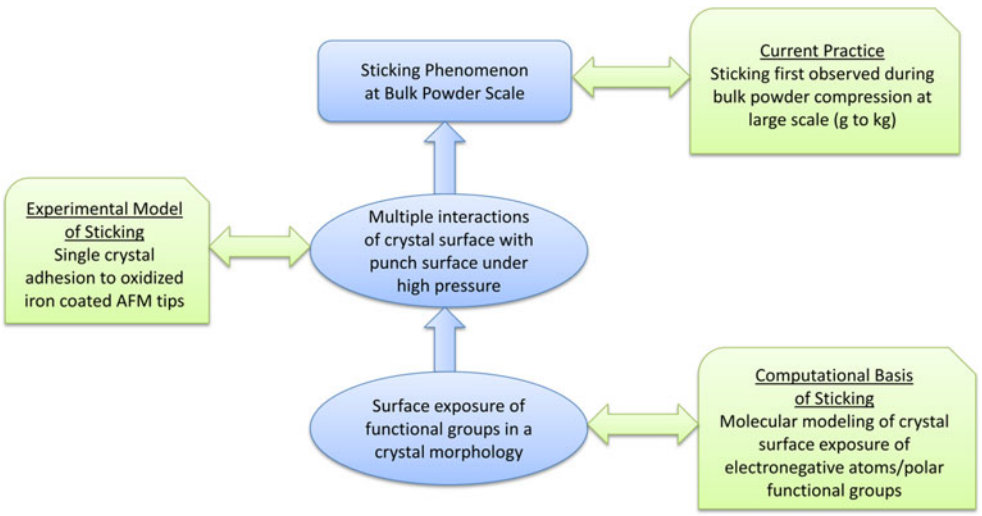

Fig. 1 Connecting crystal properties to bulk behavior in early development using material sparing techniques. The ovals highlight the underlying basis of the sticking phenomenon observed at bulk powder scale. The side boxes represent the current experimental model and computational basis proposed in this manuscript to assess the risk of sticking early in drug development.

with hexane, dried in a vacuum chamber, and stored in tightly closed containers at room temperature.

Single Crystal X-ray Diffraction

Single crystal X-ray diffraction data of MA was collected on a Bruker AXS SMART APEX CCD diffractometer. The X-ray generator was operated at 50 kV and 35 mA using MoK_α radiation. Data was collected with a ω scan width of 0.3°. A total of 606 frames per set were collected in three different settings of φ (0°, 90° and 180°) keeping the sample to detector distance of 6.03 cm and the 2θ value fixed at −25°. The data was reduced using SAINTPLUS and an empirical absorption correction was applied using SADABS (16). The crystal structure was solved by direct methods using SIR92 and refined by full matrix least squares using SHELXL97 (17,18).

Scanning Electron Microscopy

Scanning electron microscopy (SEM) images were collected on samples mounted on aluminum stubs to which adhesive carbon conductive pads had been applied. They were sputter coated using a Pelco SC-7 Auto Sputter Coater equipped with a platinum target (Ted Pella, Inc., Redding, CA). Secondary electron images were acquired at 2 kV using an FEI XL-30 FEG SEM (FEI Electron Optics, Eindhoven, The Netherlands).

Powder X-ray Diffraction

About 200 mg of samples of two morphologies were packed into a flat PXRD sample holder. The sample was tranferred to a PANalytical MPD unit (45 KV, 40 mA, Cu Kα) (PANalytical, Almelo, The Netherlands). Data were collected at room temperature in the 2 to 32 two-theta range (continuous scanning mode, scanning rate 0.03 degrees/sec). The PXRD patterns of both morphologies were compared with the simulated PXRD pattern of MA form I, which was calculated based on single crystal structure obtained from Cambridge Structure Database (CSD) (19).

Particle Size Distribution

Malvern Mastersizer 2000 (Malvern, Worcestershire, UK) instrument with dry Scirocco dispersion system was used to measure the particle size distribution (PSD). A dispersion pressure of 3 bars, gate opening of 6 mm, feeding vibration intensity of 70%, sample size of 1 g, refractive index 1.52+0.1i, and general calculation model with normal sensitivity were used. The reported results are based on volume PSD.

Atomic Force Microscopy

MA crystals were mounted onto silicon wafers. In order to assure reliable attachment of the crystal, the Si-wafers were modified by thin chemisorbed layer of poly (glycidylmethacrylate) (PGMA, 2 $mg.m^{-2}$) (20). Contact mode AFM tips (VistaProbes, Nanocience Instruments, Inc., Phoenix, AZ; spring constant 0.1 N/m, resonant frequency 28 kHz, nominal radius <10 nm) were coated with iron metal (Fig. 2) by physical vapor deposition (sputter coating) at ThinFilms, Inc. (Hillsborough, NJ) to 200-300 Å thickness, measured by profilometer. The iron deposited AFM tips were plasma oxidized to result in oxidized iron coating on the surface. The composition of the layer of oxidized iron is unknown, but is expected to be a mixture of different oxides including FeO, Fe_2O_3, and Fe_3O_4 that are known to form as a result of plasma etching (21–23). In addition, oxides of Cr may be present as well. Adhesion of drug crystals to the oxidized iron coated AFM tips is expected to model the rusted punch tips (that generally show higher sticking tendency during tablet compression, and is attributable to drug adhesion), which are also expected to exhibit a mixture of different oxides.

The tips were tested for their probe-to-probe uniformity, integrity, and robustness of performance by scanning electron microscopy (SEM, data not shown) and reproducibility of PoF measurement against the substrate background (data not shown). The sputter coat thickness was relatively consistent across several experimental runs. The tip radius is an important parameter which greatly affects the results of the force measuremants in AFM. In order to achieve reproducible results, tip radius characterization was performed using diffraction grating TGT1 (NT-MDT Inc., Russia). The tips with the radii of 35–40 nm were selected and used in the PoF measurements.

Adhesion forces of drug crystals to AFM tips were measured by determining the pull-off forces (PoF) in the z-direction using the contact mode of the atomic force microscope. Force-distance curves (Fig. 3a) were measured to characterize the interaction of AFM oxidized iron tip with MA crystals (20). DiInnova atomic force microscope (Veeco Instruments, USA) was used. Individual force-distance curves were measured for 12 crystals for each of the needle and plate morphologies. For each crystal face, measurements were made on 121 different locations in an 11×11 matrix (Fig. 3b). All measurements were completed at 25°C and relative humidity of 35%–40%.

The PoF was measured as a minimum on deflection-distance curve subtracted from average free (suspend) tip deflection (Fig. 3a). The tip was brought into very light contact with the crystal surface (force of approx. 3 nN). The light contact on the level of 3 nN during force-distance curve acquisition was crucial in order to prevent damage of the crystal surfaces as well as to preserve tip surface. For

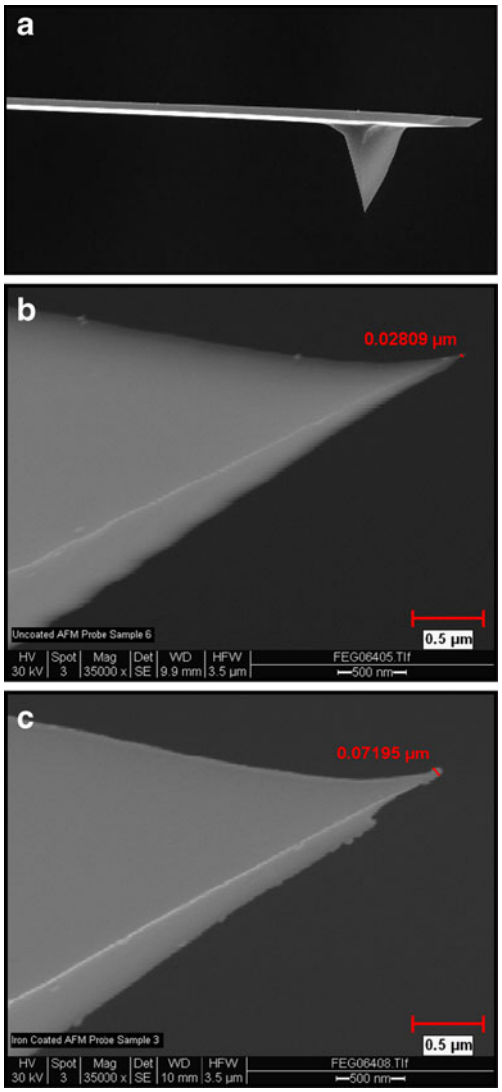

Fig. 2 Atomic force microscopy (AFM) tips. (**a**) Unmodified silicon nitride tip; (**b**) contact point or edge of the tip that touches the crystal surface; and (**c**) the contact point or edge of the tip after sputter coating with iron.

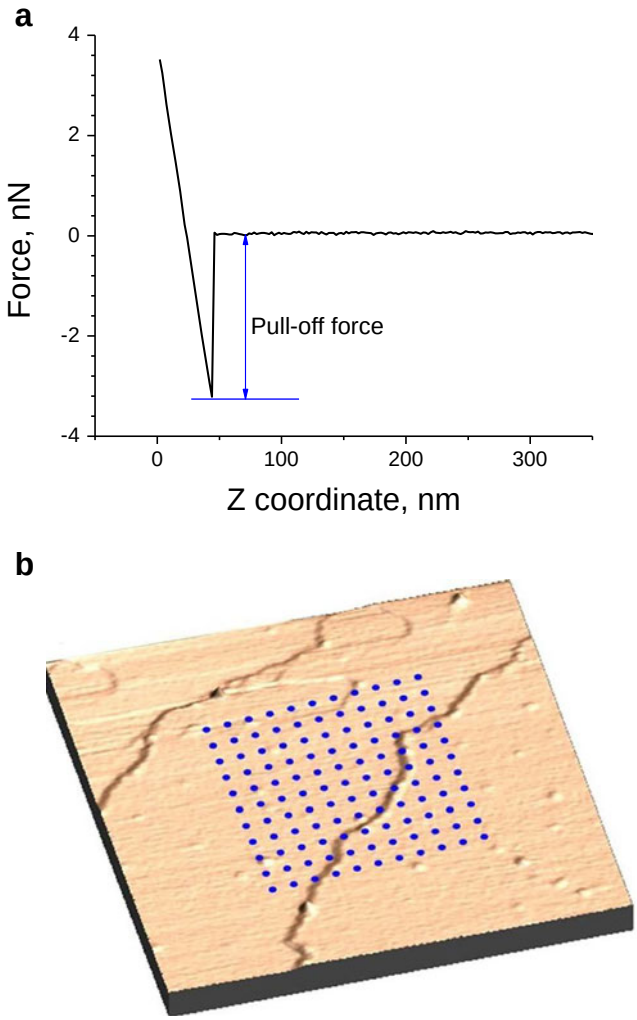

Fig. 3 A representative force-distance curve on withdraw movement ("from the surface", z increasing) obtained for a plate-like crystal of mefenamic acid (**a**) and an AFM image (tapping mode, $2 \times 2\,\mu$m) of a fragment of the plate-like crystal (3D representation) showing the schematic of acquisition of multiple force-distance curves obtained in 121 locations marked as blue dots (**b**).

comparison, contact mode scanning using same tips required about two time higher force (deflection signal 2.0 V on the scale of 0 to 10.0 V) to maintain reliable contact yet the surface remained intact. Tip deflection calibration procedure was employed routinely for each crystal.

Statistical significance of differences in PoF among the crystals of the same shape and between the two groups of different shapes of crystals was analyzed by analysis of variance (ANOVA). Two-way ANOVA was used in this study to compare significance of the source of variability in the AFM PoFs between and within the two groups of crystals. The two groups were defined as the two morphologies of mefenamic acid used in this manuscript – needles and plates. Since $n=12$ crystals were measured within each of these two groups and $n=121$ observations were recorded for each of the 12 crystals measured for the two morphologies, the data was plotted as a variability chart and mean PoFs. Variability chart (Fig. 4a) describes the mean and standard deviation of 121 data points for each of the 24 crystals. This chart also plots the mean line for each crystal morphology, which is mean of all 12x121 observations. The mean PoF data analysis (Fig. 4b) plots mean PoFs for all of the 12 crystals of each morphology. For each of the two morphologies, mean is represented as the central line in the corresponding diamond and the vertical span of each diamond represents 95% confidence interval. Statistical significance was inferred at $p<0.05$.

Morphology Modeling, Surface Energy Calculation, and Surface Functional Group Orientation

The crystal structure (.cif file) for MA was obtained from the Cambridge Structural Database (CSD) (CSD,UK), REFCODE "XYANAC" (24). The morphology simulation and analysis

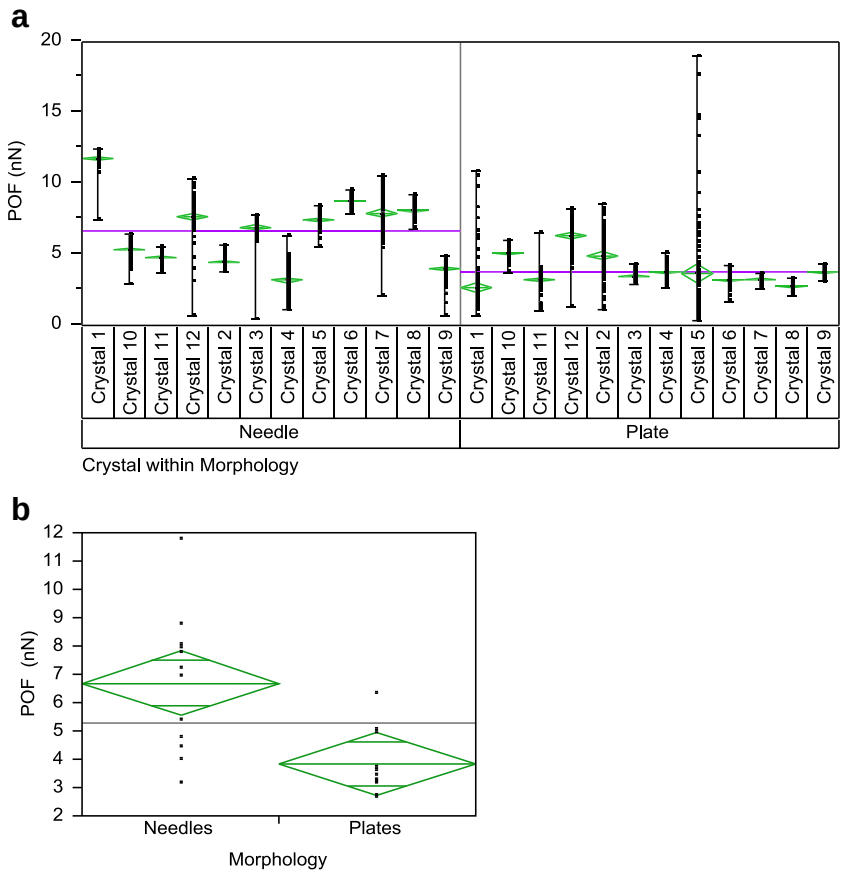

Fig. 4 Pull-off force (PoF) measurements for 12 different crystals of needle- or plate-shaped morphology by atomic force microscopy (AFM) using iron oxide coated tips. (**a**) Variability chart for PoF for $n = 121$ measurements on each individual crystal in an 11×11 matrix and (**b**) plot of PoF measurements by morphology. The variability chart (**a**) includes a horizontal line across all 12 crystals of each morphology separately indicating overall mean for each morphology. The vertical lines for each crystal represents the range and the small horizontal green line for each crystal represents the mean of measured values for the crystal. Data points are plotted on the vertical line. The analysis chart (**b**) groups the $n = 12$ crystals each by morphology plotting a diamond around a central line, which represents the group mean of the respective morphology. The vertical span of each diamond represents the 95% confidence interval for each group. The smaller horizontal lines closer to the edges of the diamonds indicate overlap marks of the two distributions. The overlap marks are an indication of statistical significance of data and are computed as group mean $\frac{\sqrt{2}}{2} \times \frac{confidence\ \ interval}{2}$. If the overlap marks in one diamond are no closer to the mean of another diamond than that diamond's overlap marks, as in this figure, it indicates that the two groups are statistically significantly different at the given confidence level ($\alpha = 0.05$).

were performed using *Morphology*, which is integrated in the simulation package *Materials Studio* version 5.5 (Acclerys Inc., San Diego, CA, USA). The structure file was loaded into the program followed by building the crystal structure. The structure was verified to be chemically correct. This crystal structure was used for all calculations without any further structure optimization. Crystal morphology was modeled by minimizing surface energy calculated for both (a) equilibrium and (b) growth morphology of the crystal based on the theory and underlying equations used for morphology prediction (25–27).

To calculate the crystal morphologies, two different force fields (FF) - COMPASS (forcefield charges and gasteinger charges) and Dreiding (gasteinger charges and model assigned) were applied to non-geometry optimized Bragg structures. A minimum d_{hkl} of 1.300 Å and a maximum value for the three Miller indices was set to 3,3,3, respectively (medium setting on the module). The overall number of growing faces was limited to 200. Applicability of the forcefield was evaluated by the similarity of the predicted morphology to experimentally observed morphology. The impact of force field on either attachment energy or predicted morphologies was minimal. Thus, the predicted morphology did not significantly depend on the forcefield used for morphology prediction. This was consistent with the observations of Brunsteiner and Price (28), who observed that the theoretical morphologies of several compounds, such as ε-caprolactam, urea, pentaerythritol, and hexamethylene tetraamine, were not significantly affected by the attachment energy model used to calculate them. Cuppen *et al.* (29) also reported lack of impact of force field on observed morphology. The parameters used in morphology calculation are summarized in Table I. Plate shaped morphology resulted in all simulations. The shapes and aspect ratios of the predicted faces were in good agreement using different force fields, indicating that, under equilibrium conditions,

plate-shaped morphology is the most stable morphology. Dreiding forcefield applied with input model-based charge assignment method (Table III) was used to predict the morphology simulated in Fig. 5a, compared with experimentally obtained morphologies in Fig. 5b. The predicted morphologies were also in agreement with the experimentally observed crystal morphologies using THF as the solvent and slow evaporation method.

For surface energy (equilibrium morphology) calculations, Dreiding forcefield, which has wide applicability across different systems, was used (26). Input model based charges without geometry optimization of the crystal structure was utilized. This equilibrium morphology feature allows for a better understanding of the ideal morphology of MA and its surface group orientations. To obtain surface energies for the needle-shaped morphology, which was observed experimentally, modification of equilibrium plate-shaped morphology was done by altering the crystal's aspect ratios within the energy constraints of the structure.

Surface functional group orientations were viewed from the standard parameter table and by expanding a particular face of the crystal using the "create super cell" function of the module.

Adhesion During Compaction

Recrystallized API was used to prepare compacts using 5/16" flat faced round tooling on a Carver hydraulic press (Carver, Wabash, IN). Each compaction was preceded by a punch cleaning and polishing step to ensure punch surface smoothness. The samples of both needle and plate morphologies were compacted on the same day. A force of 1 ton and 10 min dwell time was used with external lubrication of the die wall using magnesium stearate. After each compaction experiment, an assessment of sticking was done by visual examination.

RESULTS AND DISCUSSION

Recrystallization

Plate-shaped crystals (Fig. 5b(i)) were obtained from THF by solvent evaporation. Needle-shaped crystals (Fig. 5b(ii)) were obtained using anti-solvent (hexane) addition to a 1:1 mixture of THF and EtOH. Crystal surfaces are generally anisotropic due to the differences in the surface exposure of functional groups arising from their ordered structure in the crystal lattices. In addition, crystallization conditions (such as the solvent(s) used for crystallization) frequently result in differences in relative growth rate of different planes, leading to different morphologies of the crystals. Furthermore, the polarity and protic nature of the solvent used for crystallization influences the relative growth rate of crystal faces and determines surface exposure of functional groups on the predominant face(s).

Among the solvents used for the crystallization of MA, EtOH is more polar than THF. The dielectric constant of THF and EtOH is 7.6 and 24.6, respectively. A 1:1 v/v mixture of THF and ethanol is expected to have a dielectric constant of 16.1 by the weighted average method (30), without correcting for the intermolecular interactions between the two solvents. Higher polarity of EtOH is also evident by its higher polarity index (5.2) compared to that of THF (4.0). Polarity index of a solvent is a relative measure of the degree of

Table I Parameters Used in the Calculation of Surface Morphology of Mefenamic Acid Crystals for Both Equilibrium and Growth Morphology Methods. Plate Shaped Morphology Resulted in all Simulations.

Method	Forcefield	Charges	Total lattice energy (E_{tot}) kcal/mol	Van der Waals contribution (E_{VdW})	Electrostatic contribution (E_{ES})	Hydrogen bonding contribution (E_{Hbond})	Aspect Ratio	Number of unique facets
Attachment energy	DREIDING	Input model	−59.461	−52.062	0.000	−7.399	6.270	6
		Gasteiger (Gast)	−61.837	−52.062	−2.376	−7.399	4.913	5
	COMPASS	Force field (FF) assigned	−41.925	−44.785	2.860	0.000	4.110	5
		Gasteiger (Gast)	−47.161	−44.785	−2.376	0.000	2.840	4
Surface energy	DREIDING	Input model	−59.461	−52.062	0.000	−7.399	3.258	23
		Gasteiger (Gast)	−61.837	−52.062	−2.376	−7.399	2.626	32
	COMPASS	Force field (FF) assigned	−41.925	−44.785	2.860	0.000	2.179	43
		Gasteiger (Gast)	−47.161	−44.785	−2.376	0.000	1.733	83

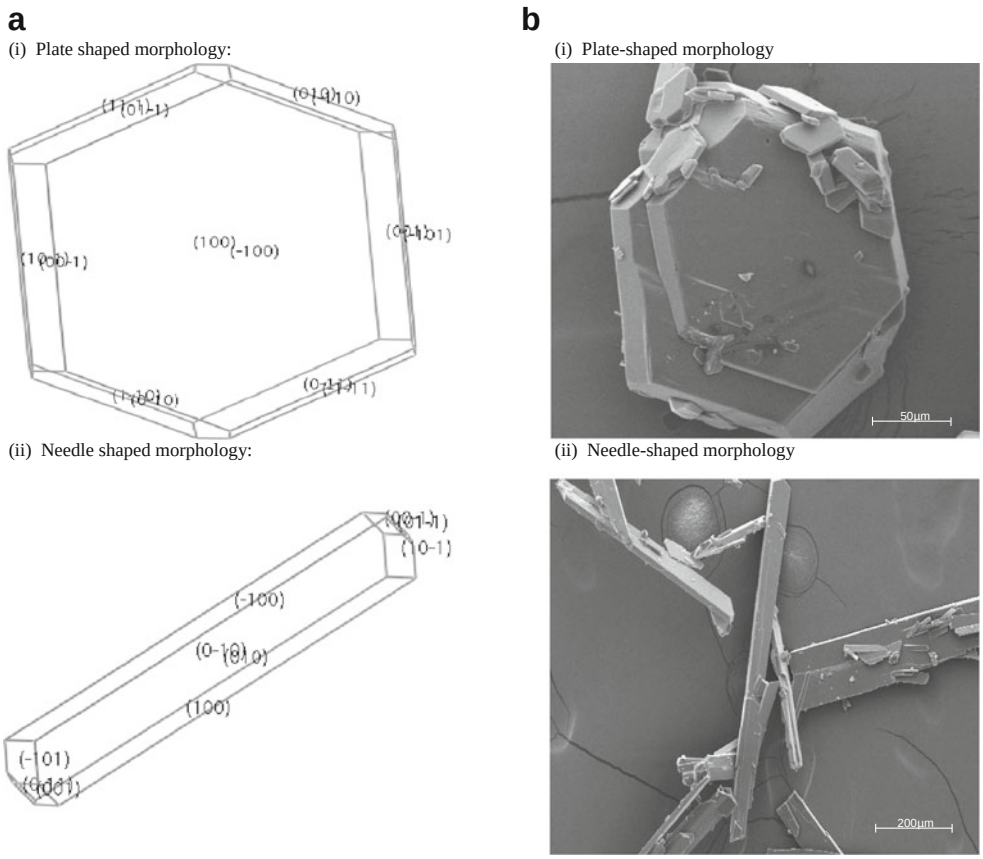

Fig. 5 (**a**) Simulation of surface crystal morphology using morphology module of Material Studio software. (**b**) Scanning electron microscopy (SEM) images of the plate and needle shaped morphologies obtained by varying the crystallization conditions.

interaction of the solvent with various polar test solutes. Higher the interaction of a solvent with polar test solutes, greater the polarity index of the solvent (31). In addition, THF is aprotic, whereas EtOH is a protic solvent. Therefore, the solvent system used for the preparation of needles was protic and more polar than the one used for the preparation for plates.

Generally, the influence of polarity and protic nature of the solvent, through its potential to interact with exposed functional groups in different planes of crystal lattice, implies that dominating crystal faces produced from polar and protic solvents are likely to be more polar compared to the crystal faces produced from aprotic solvent with lower polarity (3,4,6–8). Plate-shaped crystals of MA were produced when an aprotic solvent (THF) was used for crystallization. The use of ethanol in addition to THF in the solvent system for crystallization led to the formation of needle-shaped crystals. Ethanol being a protic solvent and a relatively more polar solvent system (THF + EtOH) resulting in needle-shaped crystals indicated that needle-shaped crystals have a greater proportion of surface that is relatively more polar and capable of hydrogen bonding. Therefore, needle-shaped crystals would be expected to have greater surface exposure of polar groups. This is consistent with molecular modeling results (discussed in "X-ray Diffraction and Morphology Simulation") and propensity for specific interactions with oxidized iron coated AFM probe tips (discussed in "Atomic Force Microscopy").

X-ray Diffraction and Morphology Simulation

MA exists in two polymorphic forms – form I and form II, of which form I is the thermodynamically more stable form at ambient conditions of temperature and pressure (32). Form I was used in these studies. Since different polymorphic forms can be generated by recrystallization under different conditions, PXRD was utilized to confirm that both plate- and needle-shaped crystals were of the same polymorphic form. PXRD patterns of recrystallized MA of both morphologies were compared with the simulated PXRD pattern for form I (Fig. 6). The PXRD studies indicated that both needles and plates are the same polymorphic form of the API.

In addition, single crystal XRD was used to confirm the Miller indices of the external faces for the plate- and needle-shaped crystal morphologies. MA form I crystallizes in a triclinic unit cell system with P-1 space group. The major face was (100) in the plate-shaped morphology. The needle shaped morphology had a much diminished face (100), while face (010) was predominant (Table II).

Equilibrium morphology calculations revealed that the plate-shaped morphology was the equilibrium morphology. Needle-shaped morphology was simulated by altering the crystal's aspect ratios within the energy constraints of the structure. The aspect ratio of the projections for both morphologies (Fig. 5) was measured using different force field and

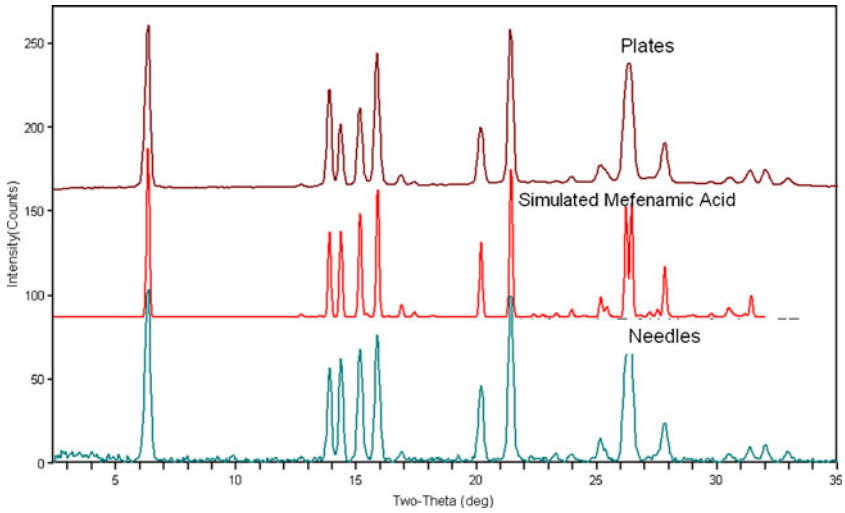

Fig. 6 Powder x-ray diffraction (PXRD) patterns for recrystallized samples of mefenamic acid compared to simulated mefenamic acid form I.

charge assignment methods. This data is summarized in Table III. This data indicated that the calculated morphologies by different methods resulted in prediction that was close to experimentally observed morphologies. The aspect ratio for observed morphologies was 2.6 for the plate-shaped morphology and 9.4 for the needle-shaped morphology, obtained by measuring several crystals of each morphology.

Faces of plate- and needle-shaped morphologies were identified based on the combined single crystal XRD and Material Studio simulation results. The simulation further indicated the surface orientation of the molecules on different faces, as shown in Fig. 7. Face (100) consisted of predominantly nonpolar hydrocarbon groups, with the hydrophilic amine and carbonyl groups occurring less frequently and buried deeper into the surface compared to the other faces (001) and (010).

The molecular modeling simulation indicated that the plate-shaped morphology has a significantly higher surface area contribution from the relatively hydrophobic face (100) compared to the needle-shaped morphology. These simulations are based on attachment energy calculations. The growth rate of a particular face is proportional to the magnitude of the attachment energy between drug molecules, *i.e.*, the energy that would be reduced by the attachment of a slice of crystalline drug molecules on the growing crystal surface. Thus, the face with the lowest attachment energy is the slowest growing face, which thereby becomes the morphologically dominant face in the crystals. These results are also consistent with the expectation based on surface interaction of MA molecules during crystallization with the solvent(s) used for crystallization, as discussed in "Recrystallization".

Table II Surface Energy of Different Faces Calculated by the Morphology Module of the Accelrys Material Studio Software. Dreiding Forcefield with Input Model Based Parameters Were Used.

Face	Surface energy ($kcal \bullet mol^{-1} \bullet Å^2$)	% Facet area[a]	
		(plates)	(needles)
(100)	0.045	45	24.1
(001)	0.134	0.45	2.2
(010)	0.083	13.6	70.5
(01–1)	0.085	11.0	
(10–1)	0.15	1.2	
(1–11)	0.076	11.0	
(1–10)	0.090	5.4	
(101)	0.103	6.7	

[a] Both morphologies have additional faces (account for % facet area ≤ 1%) that are not included to maintain clarity of discussion; needles lack the unique number the of faces that plates possess.

Atomic Force Microscopy

Adhesion forces of drug crystals to AFM tips were measured by determining the PoF for 12 crystals of each morphology and 121 locations per crystal on the randomly exposed face to allow for statistical data treatment. Ideally, AFM PoF measurements on the same single crystal that was used for face indexing by single crystal X-ray diffraction would allow identification of PoF for specific crystal faces. However, this approach was logistically difficult. Therefore, we ran multiple

Table III Aspect Ratio of the Projections for the Two Morphologies Using Different Force Field and Charge Assignment Methods.

Forcefield	Charge assignment method	Aspect ratio for the two morphologies	
		Plate-shaped	Needle-shaped
DREIDING	Gasteinger	2.63	8.80
	Input model-based	3.26	7.74
COMPASS	Gasteinger	1.73	8.03
	Force field	2.18	10.67

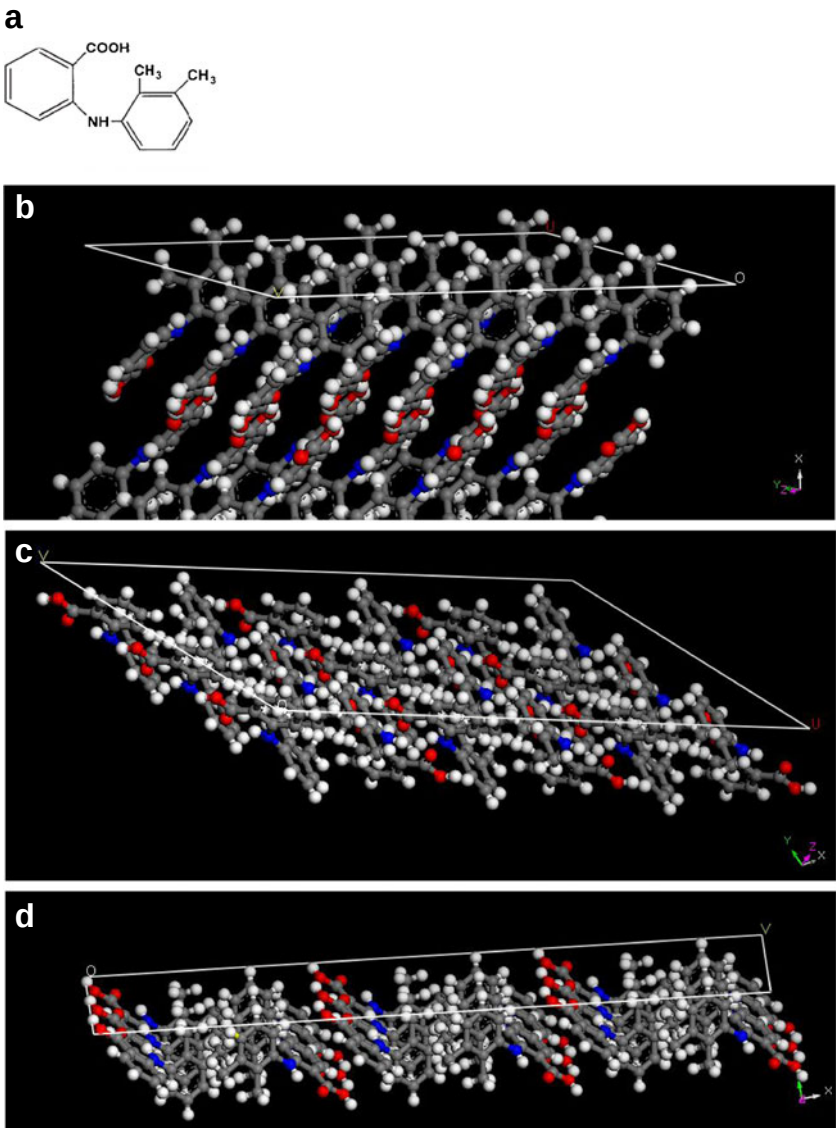

Fig. 7 Surface group orientation differences depicted at different facets of the morphology. The surface exposure of electronegative atoms/functional groups on different faces are evident by the plane drawn with white lines in the sub-figures. The following notations of atoms are used in these drawings: grey, carbon; white, hydrogen; blue, nitrogen; and red, oxygen. Dreiding forcefield with input model based parameters were used. (**a**) Chemical structure of mefenamic acid. (**b**) Surface exposure of electronegative atoms/functional groups on face (100). This face shows the presence predominantly of methyl substituents on the benzene ring on the surface. (**c**) Surface exposure of electronegative atoms/functional groups on face (001). This face shows the presence predominantly of benzene rings on the surface. (**d**) Surface exposure of electronegative atoms/functional groups on face (010). This face shows the presence predominantly of nitrogens and the oxygens on the surface, intermittently with the methyl groups.

AFM measurements across different faces of several crystals. Statistical approach was taken to overcome the limitation from the difficulty in indexing exact faces that are measured in AFM. Several ($n=12$) crystals were measured for each morphology at multiple locations (121 measurements for each crystal), and statistical methodology was utilized to quantify overall differences between the two morphologies. The PoF values for each crystal analyzed for both morphologies were plotted, as shown in Fig. 4a, and mean PoF for all 12 crystals of each of the two morphologies were plotted (Fig. 4b). Two-way ANOVA analysis indicated that the predominant source of variability in the PoF data was the difference in the morphology ($p<0.005$).

The PoFs for needles were generally higher than that for plates. As discussed earlier, the overall crystal surface of needles is expected to be more polar than plates based on molecular modeling simulations and the relative characteristics of the solvents used for crystallization of the two morphologies. Thus, the morphology with greater surface polarity showed higher adhesion to oxidized iron coated AFM tips. This was consistent with the proposed hypothesis of stronger polar surface interactions being involved in the interaction with oxidized metal on punch surfaces contributing to the crystal surface adhesion leading to the sticking phenomenon.

Adhesion Behavior During Tableting

Tableting of recrystallized MA indicated differences in the adhesive nature of the two morphologically different materials. Needles appeared to have a higher tendency to adhere to punch face compared to plates (Fig. 8). The tableting studies were carried out at 1 ton pressure and 10 min dwell time. The use of higher dwell time was designed to prolong the duration of contact between the drug and the punch surface under high

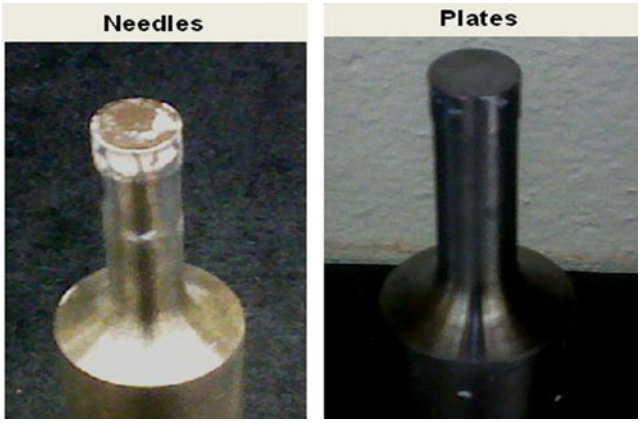

Fig. 8 Effect of morphology on the sticking tendency of needles and plates to tablet tooling punches during compression.

pressure, trying to simulate the impact of multiple punch hits usually associated with the first observation of the phenomenon of sticking in large scale tablet manufacture.

Sticking behavior is empirically related to several formulation and processing variables such as the API particle size and surface area, granulation state of API particles, particle coating with a hydrophobic agent such as magnesium stearate (lubrication), moisture content of the formulation, ambient humidity during processing, contact time and pressure between the drug and the steel surface, radius of curvature of the punches (in the case of tablet manufacturing), and the roughness of the steel surface (13,15,33–38). All these parameters were kept approximately constant for comparing the relative sticking behavior of the two morphologies. In addition, the crystallization conditions were selected to result in similar PSD of the two crystal morphologies (Fig. 9).

Anisotropy in the crystal growth planes between the two morphologies and the corresponding differences in the surface attachment energies of the two crystal morphologies correlated better with the bulk powder observation of sticking. The sticking phenomenon is expected to correlate to the surface energy of a crystal morphology. The surface energy of a crystal can be mathematically computed to reflect different parameters – such as maximum of any facet, mean, median, surface weighted mean, or surface normalized mean. Since the sticking phenomenon usually involves multiple punch hits, the surface energy of the predominant face of the crystal is identified as a key contributing factor to the sticking phenomenon. The contribution to the sticking phenomenon from facets that represent minor proportion of the crystal surface area is expected to be minimal. Therefore, avoiding any mathematical transformation of the surface energy values, Table II lists the surface energy of predominant faces of the two morphologies. Morphology modeling studies indicated that (100) was the largest face of the plate-shaped morphology, and that this face had relatively minor contribution to the overall surface area in the needle shaped morphology (Fig. 5a). The face (010) is predominant in needles (70.5% of surface area) compared to plates (19.7% of surface area) (Table II).

Surface group orientation of functional groups on different faces (Fig. 7) indicated that the face (100) is relatively nonpolar compared to the other two faces (001) and (010). As seen in Fig. 7, faces (001) and (010) had substantially higher surface exposure of nitrogen and oxygen atoms, compared to the face (100) – which has significant surface exposure of carbons and hydrogens.

These observations were in good agreement with the surface energy of different faces calculated using the Morphology module of the Accelrys Material Studio software (Table II). The surface energy of face (100) was significantly lower (0.045 kcal•mol^{-1}•Å^{2}) compared to that of the face (001) (0.134 kcal•mol^{-1}•Å^{2}) and face (010) (0.083 kcal•mol^{-1}•Å^{2}).

Fig. 9 Particle size distribution for both morphologies of MA.

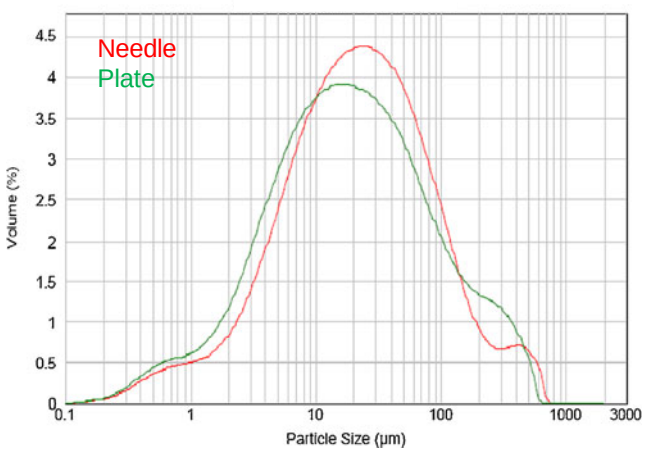

	D(0.1) µm	D(0.50) µm	D(0.90) µm	D(0.95) µm	D(3,2)
Needles	3.4	21.8	119.2	208.3	6.4
Plates	2.6	18.4	142.7	247.7	5.4

The surface energy indicates the energy released upon the attachment of a growth slice to a growing crystal face (39), or the energy required for the disruption of intermolecular bonds when a layer is removed. Thus, surfaces that have strong intermolecular bonds, such as due to polarity introduced by electronegative atoms, would have higher surface energy. The surface energy enables the identification of polar faces in anisotropic crystals (40). Higher surface energy is associated with greater polarity of the face. Therefore, the results of molecular modeling indicated that the face (100) is relatively nonpolar or hydrophobic compared to the other two faces, and greater surface polarity of the needle-shaped morphology. Thus, higher sticking tendency of needles can be largely associated with greater surface polarity of needle-shaped morphology. This is supported by greater interaction of polar surface with metals in the processing equipment, such as tablet punches.

Greater adhesion of needle-shaped crystals, with greater surface polarity, is consistent with the obervations of Podczeck, who observed that the surface interaction and adhesion of pregelatinized starch and lactose to metal modified stainless steel surfaces increased with the increasing Lewis-base, polar, character of the surfaces (41). The adhesion tendency was the least for chromium nitride, which provides a non-polar surface; whereas it was higher for steel, carbon, and chromium carbide surfaces – which are strong Lewis-bases.

CONCLUSIONS

This work showed the correlation of macro- or bulk-powder scale adhesion properties of two morphologically different forms of an API to its micro-scale crystal morphology through surface modeling, surface energy calculation, and AFM surface characterization (Fig. 1). The needle-shaped morphology of MA showed higher sticking tendency to steel punch surface during compaction, compared to plates. The higher sticking tendency of the needles correlated with their greater surface polarity, which was evident in surface energy calculations, and was attributable to the greater surface exposure of electronegative atoms and the polar functional groups. This finding is consistent with the hypothesis of adhesion behavior being attributable to specific, stronger interactions due to the surface exposure of electronegative atoms. In addition, AFM studies using oxidized iron coated tips indicated greater PoF for needles compared to plates, which correlated well with the higher surface polarity of needles.

The correlation of mean crystal surface adhesion to oxidized iron coated tips by AFM to sticking observations during tableting indicates that AFM can be used as an experimental tool to assess surface energy and prospectively assign a risk of sticking to new drug molecules in development. The bulk powder stage properties, such as sticking, often become evident only at larger scale of operation. However, unlike excipients, limited quantity of API is available in early stages of drug development. Thus, the sticking behavior, often compromising drug product manufacturability, becomes evident only in the later stages in drug development, affecting project timelines and drug development costs. Use of API sparing characterization techniques in early development, such as AFM and single crystal X-ray diffraction coupled with molecular modeling and surface energy calculation, could play a critical role in identifying high risk APIs earlier in development as well as providing guidance to the selection of appropriate form and morphology.

ACKNOWLEDGMENTS AND DISCLOSURES

Authors thank David Wantuch and Anisha Patel for their help with PXRD; Michael Galella for single crystal X-ray diffraction analysis; Eric Chan for surface energy calculations; Nigora Issamidinova and Mario Hubert for PSD and SEM analyses; and Lynn DiMemmo and Sarah DeLeon for SEM.

REFERENCES

1. Nada AH, Al-Saidan SM, Mueller BW. Crystal modification for improving the physical and chemical properties of ibuprofen. Pharm Technol. 2005;29:90–4. 100–1.
2. Rasenack N, Muller BW. Ibuprofen crystals with optimized properties. Int J Pharm. 2002;245:9–24.
3. Rasenack N, Muller BW. Properties of ibuprofen crystallized under various conditions: a comparative study. Drug Dev Ind Pharm. 2002;28:1077–89.
4. Nokhodchi A, Bolourtchian N, Dinarvand R. Crystal modification of phenytoin using different solvents and crystallization conditions. Int J Pharm. 2003;250:85–97.
5. Beckmann W. Nucleation phenomena during the crystallization and precipitation of Abecarnil. J Cryst Growth. 1999;198/199:1307–14.
6. Wang WS, Aggarwal MD, Choi J, Gebre T, Shields AD, Penn BG, *et al.* Solvent effects and polymorphic transformation of organic nonlinear optical crystal L-pyroglutamic acid in solution growth processes. I. Solvent effects and growth morphology. J Cryst Growth. 1999;198/199:578–82.
7. Holmback X, Rasmuson AC. Size and morphology of benzoic acid crystals produced by drowning-out crystallization. J Cryst Growth. 1999;198/199:780–8.
8. Braybrook AL, Heywood BR, Karatzas P. An experimental investigation of crystal/solvent interactions in the copper (II) acetate monohydrate/propan-1-ol system. J Cryst Growth. 2002;244:327–32.
9. Heng JY, Bismarck A, Lee AF, Wilson K, Williams DR. Anisotropic surface chemistry of aspirin crystals. J Pharm Sci. 2007;96:2134–44.
10. Heng JY, Bismarck A, Williams DR. Anisotropic surface chemistry of crystalline pharmaceutical solids. AAPS PharmSciTech. 2006;7:84.
11. Danesh A, Connell SD, Davies MC, Roberts CJ, Tendler SJ, Williams PM, *et al.* An in situ dissolution study of aspirin crystal planes (100) and (001) by atomic force microscopy. Pharm Res. 2001;18:299–303.

12. Eve JK, Patel N, Luk SY, Ebbens SJ, Roberts CJ. A study of single drug particle adhesion interactions using atomic force microscopy. Int J Pharm. 2002;238:17–27.
13. Bunker M, Zhang J, Blanchard R, Roberts CJ. Characterising the surface adhesive behavior of tablet tooling components by atomic force microscopy. Drug Dev Ind Pharm. 2011;37:875–85.
14. Wang JJ, Li T, Bateman SD, Erck R, Morris KR. Modeling of adhesion in tablet compression–I. Atomic force microscopy and molecular simulation. J Pharm Sci. 2003;92:798–814.
15. Adam A, Schrimpl L, Schmidt PC. Some physicochemical properties of mefenamic acid. Drug Dev Ind Pharm. 2000;26:477–87.
16. Software SHELXTL. Bruker AXS Inc., Madison, WI; 1998.
17. Altomare A, Cascarano G, Giacovazzo C, Guagliardi A. Completion and refinement of crystal structures with SIR92. J Appl Crystallogr. 1993;26:343–50.
18. Sheldrick G. A short history of SHELX. Acta Crystallogr A. 2008;64:112–22.
19. Cambridge Structure Database (CSD). Cambridge Crystallographic Data Centre. http://www.ccdc.cam.ac.uk/products/csd/ (accessed August 29, 2012).
20. Enright TP, Hagaman D, Kokoruz M, Coleman N, Sidorenko A. Gradient and patterned polymer brushes by photoinitiated "grafting through" approach. J Polym Sci, Part B: Polym Phys. 2010;48:1616–22.
21. Okado J, Okada K, Ishiyama A, Setsuhara Y, Takenaka K. Corrosion resistance of plasma-oxidized stainless steel. Surf Coat Technol. 2008;202:5595–8.
22. Syed AA, Denoirjean A, Fauchais P, Labbe JC. On the oxidation of stainless steel particles in the plasma jet. Surf Coat Technol. 2006;200:4368–82.
23. Donik C, Kocijan A, Grant JT, Jenko M, Drenik A, Pihlar B. XPS study of duplex stainless steel oxidized by oxygen atoms. Corros Sci. 2009;51:827–32.
24. McConnell JF, Company FZ. N-(2,3-Xylyl)anthranilic acid, C15H15NO2. Mefenamic acid. Cryst Struct Commun. 1976;5:861–4.
25. York P, Ticehurst MD, Osborn JC, Roberts RJ, Rowe RC. Characterization of the surface energetics of milled dl-propranolol hydrochloride using inverse gas chromatography and molecular modeling. Int J Pharm. 1998;174:179–86.
26. Mayo SL, Olafson BD, Goddard III WA. DREIDING: a generic force field for molecular simulations. J Phys Chem. 1990;94:8897–909.
27. Berkovitch-Yellin Z. Toward an ab initio derivation of crystal morphology. J Am Chem Soc. 1985;107:8239–53.
28. Brunsteiner M, Price SL. Morphologies of organic crystals: sensitivity of attachment energy predictions to the model intermolecular potential. Cryst Growth Des. 2001;1:447–53.
29. Cuppen HM, Day GM, Verwer P, Meekes H. Sensitivity of morphology prediction to the force field: paracetamol as an example. Cryst Growth Des. 2004;4:1341–9.
30. Prakongpan S, Nagai T. Pharmaceutical interactions in dosage forms and processing. XLV. Solubility of acetaminophen in cosolvents. Chem Pharm Bull. 1984;32:340–3.
31. Di Martino P, Censi R, Malaj L, Capsoni D, Massarotti V, Martelli S. Influence of solvent and crystallization method on the crystal habit of metronidazole. Cryst Res Technol. 2007;42:800–6.
32. Romero S, Escalera B, Bustamante P. Solubility behavior of polymorphs I and II of mefenamic acid in solvent mixtures. Int J Pharm. 1999;178:193–202.
33. Kakimi K, Niwa T, Danjo K. Influence of compression pressure and velocity on tablet sticking. Chem Pharm Bull. 2010;58:1565–8.
34. Roberts M, Ford JL, MacLeod GS, Fell JT, Smith GW, Rowe PH, *et al.* Effect of punch tip geometry and embossment on the punch tip adherence of a model ibuprofen formulation. J Pharm Pharmacol. 2004;56:947–50.
35. Roberts M, Ford JL, MacLeod GS, Fell JT, Smith GW, Rowe PH, *et al.* Effect of lubricant type and concentration on the punch tip adherence of model ibuprofen formulations. J Pharm Pharmacol. 2004;56:299–305.
36. Roberts M, Ford JL, MacLeod GS, Fell JT, Smith GW, Rowe PH. Effects of surface roughness and chrome plating of punch tips on the sticking tendencies of model ibuprofen formulations. J Pharm Pharmacol. 2003;55:1223–8.
37. Kim JS, Lotz B, Lindrud M, Girard KP, Moore T, Nagarajan K, *et al.* Control of the particle properties of a drug substance by crystallization engineering and the effect on drug product formulation. Org Process Res Dev. 2005;9:894–901.
38. Yin SX and Grosso JA. Selecting and Controlling API Crystal Form for Pharmaceutical Development: Strategies and Processes. Curr Opin Drug Discovery Develop. 2008;11:771–7.
39. Docherty R, Clydesdale G, Roberts KJ, Bennema P. Application of Bravais-Friedel-, I Donnay-Harker, attachment energy I and king models to predicting and understanding the morphology of molecular crystals. J Phys D: Appl Phys. 1991;24:89–99.
40. Clydesdale G, Roberts KJ, Telfer GB, Saunders VR, Pugh D, Jackson RA, *et al.* Prediction of the polar morphology of sodium chlorate using a surface-specific attachment energy model. J Phys Chem B. 1998;102:7044–9.
41. Podczeck F. Investigations into the reduction of powder adhesion to stainless steel surfaces by surface modification to aid capsule filling. Int J Pharm. 1999;178:93–100.